



CHALMERS
UNIVERSITY OF TECHNOLOGY

Indenocarbazole and benzofurocarbazole-based bipolar host materials for high-performance red and green Phosphorescent Organic Light-Emitting

Downloaded from: <https://research.chalmers.se>, 2025-06-07 16:45 UTC

Citation for the original published paper (version of record):

Li, M., Yang, Y., Lan, S. et al (2025). Indenocarbazole and benzofurocarbazole-based bipolar host materials for high-performance red and green Phosphorescent Organic Light-Emitting Diodes. *Dyes and Pigments*, 241. <http://dx.doi.org/10.1016/j.dyepig.2025.112882>

N.B. When citing this work, cite the original published paper.



Indenocarbazole and benzofurocarbazole-based bipolar host materials for high-performance red and green Phosphorescent Organic Light-Emitting Diodes

Minzhen Li^a, Yong Yang^a, Sisi Lan^b, Yingyi Wei^b, Zhi Zhang^b, Haitao Zhou^{c,**}, Zhiyun Zhang^a, Jinhai Huang^c, Zhenyuan Xia^{d,*}

^a Key Laboratory for Advanced Materials and Institute of Fine Chemicals, East China University of Science & Technology, #130 Meilong Road, Shanghai, 200237, PR China

^b College of Ecology, Lishui University, Lishui, Zhejiang, 323000, PR China

^c Shanghai Taoe Chemical Technology Co., Ltd, Shanghai, PR China

^d Industrial and Materials Science, Chalmers University of Technology, Hörsalsvägen 7B, Göteborg, Sweden

ARTICLE INFO

Keywords:

Indolocarbazole
Benzofurocarbazole
Bipolar host materials
Phosphorescent organic light-emitting diodes
Hole-transporting properties

ABSTRACT

In this research, two innovative bipolar host materials, **DMID-BP** and **BFCz-BP**, were strategically designed and synthesized, marking the first application of these materials in red and green phosphorescent organic light-emitting diodes. Both compounds exhibit remarkable bipolar carrier transport properties, well aligned HOMO and LUMO levels, and exceptional thermal stability, with T_g value of 185 °C and 171 °C, respectively. The red and green Phosphorescent Organic Light-Emitting Diodes (PhOLEDs) fabricated with these two materials demonstrate high light-emitting efficiency along with low efficiency roll-off. Notably, R1 device, utilizing **DMID-BP** as the host material, achieves an impressive maximum external quantum efficiency (EQE_{max}) of 23.68 %, significantly surpassing most conventional host materials reported to date. Additionally, the R2 device, based on **BFCz-BP**, also attains a high EQE_{max} of 20.26 %. Consequently, all the results underscore the significant potential of these two host materials for applications in both red and green PhOLEDs.

1. Introduction

Following the discovery of a semiconductor molecule that emits light under an electric field in 1987, research on organic light-emitting diodes (OLEDs) has been progressing so far [1]. Nowadays, OLEDs have drawn widespread interest because of their potential applications in solid-state illumination and full-color information display technologies [2–5]. During the electroluminescence process, electron-hole capture generates 25 % singlet and 75 % triplet excitons. However, traditional fluorescent OLEDs only use singlet excitons for light emission, leading to a very low Internal Quantum Efficiency (IQE) [6,7]. To overcome this limitation, phosphorescent OLEDs (PhOLEDs) were developed, which leverage the spin-orbital coupling effects introduced by heavy metals, enabling the harvesting of both singlet and triplet excitons and achieving a theoretical IQE of up to 100 % [8,9]. Despite this advantage, phosphorescent emitters still face challenges such as triplet-triplet annihilation (TTA)

and triplet-polaron quenching (TPQ) at high concentrations or increased luminance [10]. These issues arise from the extended lifetime of triplet excitons, thereby constraining the practical application of these materials [11–14]. Fortunately, the host-guest system has been developed to address these concerns, incorporating both electron donor (D) and acceptor (A) fragments into the emitters to confer bipolar-transporting characteristics [15,16]. In comparison to unipolar hosts, where the recombination zone within the emitting layer (EML) is often confined and shifting to the interface near the electron transport layer (ETL) or hole transport layer (HTL), bipolar hosts exhibit more balanced hole and electron transport properties that can effectively suppress the previously mentioned efficiency loss and prevent efficiency roll-off at high luminance [17–20]. Thus, a suitable host material for PhOLEDs must fulfill specific criteria: Firstly, its triplet energy level (E_T) should exceed that of the guest emitter to evade undesirable reverse energy transfer, effectively confining triplet excitons within the guest molecules.

* Corresponding author.

** Corresponding author.

E-mail addresses: haitao.zhou@163.com (H. Zhou), zhenyuan@chalmers.se (Z. Xia).

<https://doi.org/10.1016/j.dyepig.2025.112882>

Received 11 March 2025; Received in revised form 7 May 2025; Accepted 8 May 2025

Available online 8 May 2025

0143-7208/© 2025 The Authors. Published by Elsevier Ltd. This is an open access article under the CC BY license (<http://creativecommons.org/licenses/by/4.0/>).

Furthermore, it should demonstrate a high and well-balanced charge-carrier mobility to optimize electron-hole recombination. Additionally, proper alignment of the frontier molecular orbital energy levels is essential for minimizing the driving voltage. Finally, excellent thermal and morphological stability is required to extend the operational lifespan of the devices [21–23].

To fulfill these requirements, bipolar host materials featuring a donor- π -acceptor (D- π -A) structure have been rationally designed in PhOLEDs. In this structure, the π -conjugated system serves as a bridge between the hole and electron transport units to facilitate bipolar charge transfer with proper carrier balance [24]. Among the D- π -A system, donor-type carbazole structure is widely recognized as a preferred hole transport units for developing bipolar host materials, owing to its exceptional hole-transporting properties, high energy transfer (E_T) and excellent thermal stability [25]. Furthermore, acceptor units with electron-transporting property, including triazine, pyridine, and benzimidazole are commonly used in various OLEDs with high-performance [26]. However, achieving balanced charge transport is still a challenge. For example, hole mobility in hole-transport materials, especially those based on carbazole, are several orders of magnitude higher than their electron-transporting counterparts. Previous research has predominantly focused on improving electron mobility on the electron-transporting units on the D- π -A compound. However, to optimize overall device performance, it is imperative to design new hole-transporting unit that rival the efficiency of the leading electron-transporting materials. The 7,7-dimethyl-5,7-dihydroindeno [2,1-b]carbazole (DMID) unit has shown excellent potential as hole-transporting materials due to its exceptional chemical, thermal, photochemical stability, as well as its ability to minimize undesirable nonradiative emission [27,28]. Besides, the electron-donating methyl groups attached to the indolocarbazole unit slightly elevate the highest occupied molecular orbital (HOMO) level, thereby facilitating hole injection and transport in OLED devices. Similarly, benzofurocarbazole has proven to be a more effective hole-transporting moiety than carbazole, owing to the electron-donating oxygen atom in the furan ring and its superior thermal stability, both of which contribute to enhanced quantum efficiency [29,30]. Consequently, both moieties serve as potential hole-transporting material for constructing bipolar hosts with D- π -A structure. Meanwhile, benzimidazole-hybridized phenanthridine unit has recently been adopted as an electron-transport moiety owing to its demonstrated efficacy as red bipolar host materials and good thermal stability [31].

In this research, two novel bipolar host materials, 7-(4-(7,7-dimethylindeno [2,1-b]carbazol-5(7H)-yl)phenyl)benzo [4,5]imidazo [1,2-f]phenanthridine (DMID-BP) and 5-(4-(benzo [4,5]imidazo [1,2-f]phenanthridin-7-yl)phenyl)-5H-benzofuro [3,2-c]carbazole (BFCz-BP), were designed and synthesized by employing the aforementioned hole-transporting units. Both DMID-BP and BFCz-BP, demonstrate exceptional thermal stability, characterized by glass transition temperatures (T_g) exceeding 170 °C. Additionally, their high E_T and appropriate HOMO and LUMO levels further qualify them as ideal host materials for practical applications. Red and green PhOLEDs utilizing the two materials present overall outstanding electroluminescence (EL) performance. Notably, the red PhOLED hosted by DMID-BP achieved a high maximum external quantum efficiency (EQE_{max}) value of 23.68 %, probably due to its superior electron mobility.

2. Experimental section

2.1. Synthesis and characterization

2.1.1. Synthesis of 2-(4-chloro-2'-fluoro-[1,1'-biphenyl]-2-yl)-1H-benzo[d]imidazole (IN1)

4-chloro-2'-fluoro-[1,1'-biphenyl]-2-carbaldehyde (20.0 g, 85.24 mmol), benzene-1,2-diamine (11.1 g, 102.28 mmol) and sodium bisulfite (97.56 g, 937.56 mmol) were sequentially introduced in a three-

necked flask. Thereafter, 800 mL of water was poured in the flask. Then stirring the mixture to reflux under nitrogen (N_2) atmosphere for 2.5 h. After cooling, the crude product was isolated via diafiltration. Then the mixture underwent purification through column chromatography, employing silica gel as the stationary phase and a PE/DCM (5:1, v/v) mixture used for eluent, yielding 12 g of white solid with a 60 % yield.

2.1.2. Synthesis of 7-chlorobenzo [4,5]imidazo [1,2-f]phenanthridine (IN2)

IN1 (12 g, 37.18 mmol), K_2CO_3 (15.4 g, 111.54 mmol) and DMF (120 mL) were sequentially introduced in a three-necked flask. Following this, stirring the mixture to reflux under nitrogen (N_2) atmosphere for 4 h (120 °C). After cooling and filtering, the white solid product underwent purification through column chromatography, employing silica gel as the stationary phase and a PE/DCM (4:1, v/v) mixture as the eluent, yielding 10.2 g of white solid with an 89 % yield.

2.1.3. Synthesis of 5-(4-bromophenyl)-7,7-dimethyl-5,7-dihydroindeno [2,1-b]carbazole (IM1)

7,7-dimethyl-5,7-dihydroindeno [2,1-b]carbazole (10.0 g, 35.28 mmol), 1,4 dibromobenzene (33.2 g, 141.16 mmol), K_2CO_3 (14.6 g, 105.86 mmol), CuI (3.4 g, 17.64 mmol) and 200 mL DMAC were introduced in a three-necked flask respectively. Then stirring the mixture to reflux under nitrogen (N_2) atmosphere for 2 h (160 °C). After cooling and filtering, the white solid product underwent purification through column chromatography, employing silica gel as the stationary phase and a PE/DCM (5:1, v/v) mixture used for eluent, yielding 13.6 g of white solid with an 88 % yield.

2.1.4. Synthesis of 5-(4-bromophenyl)-5H-benzofuro [3,2-c]carbazole (IM2)

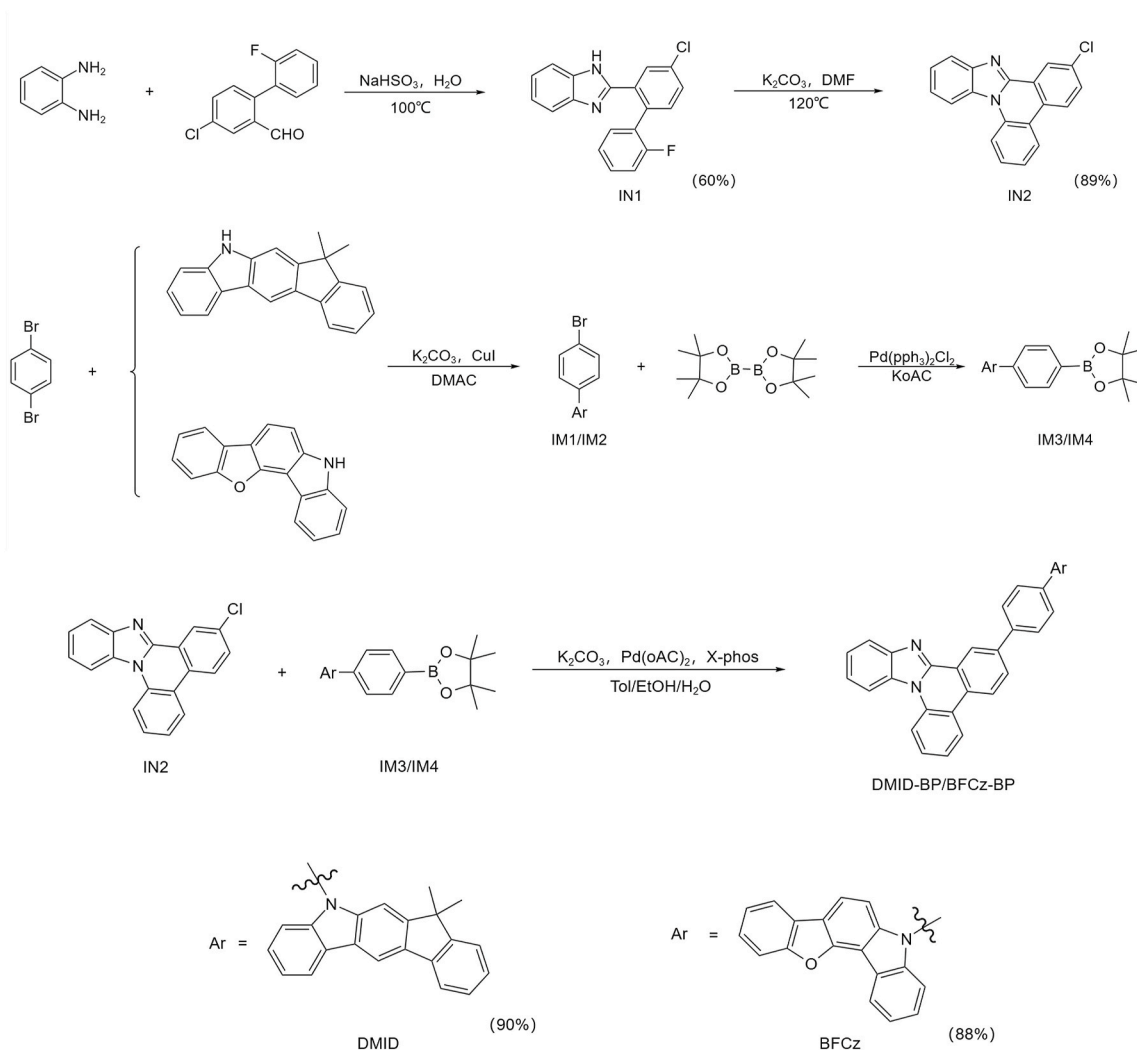
5H-benzofuro [3,2-c]carbazole (10 g, 38.86 mmol), 1,4-dibromobenzene (36.8 g, 155.56 mmol), K_2CO_3 (16.2 g, 116.58 mmol), CuI (3.8 g, 19.44 mmol) and 200 mL DMAC were introduced in a three-necked flask respectively. Then stirring the mixture to reflux under nitrogen (N_2) atmosphere for 2 h (160 °C). After cooling and filtering, the white solid product underwent purification through column chromatography, employing silica gel as the stationary phase and a PE/DCM (5:1, v/v) mixture used for eluent, yielding 13.8 g of white solid with an 87 % yield.

2.1.5. Synthesis of 7,7-dimethyl-5-(4-(4,4,5,5-tetramethyl-1,3,2-dioxaborolan-2-yl)phenyl)-5,7-dihydroindeno [2,1-b]carbazole (IM3)

In a three-necked flask, a mixture containing IM1 (13.6 g, 31.02 mmol), 4,4,4',4',5,5',5'-octamethyl-2,2'-bi(1,3,2-dioxaborolane) (9.4 g, 37.22 mmol), KOAc (6.2 g, 62.04 mmol) and Pd(PPh₃)₂Cl₂ (0.4 g, 0.58 mmol) was prepared. Redistilled toluene (200 mL) was subsequently poured in the mixture, then stirring the mixture to reflux under nitrogen (N_2) atmosphere for 5 h. Following this, the mixture was hot-filtered utilizing silica gel column and subsequently concentrated to dryness, resulting in a white solid. (11 g, 78 %)

2.1.6. Synthesis of 5-(4-(4,4,5,5-tetramethyl-1,3,2-dioxaborolan-2-yl)phenyl)-5H-benzofuro [3,2-c]carbazole (IM4)

In a three-necked flask, a mixture containing IM2 (13.8 g, 33.72 mmol), 4,4,4',4',5,5',5'-octamethyl-2,2'-bi(1,3,2-dioxaborolane) (10.2 g, 40.46 mmol), KOAc (6.6 g, 67.42 mmol) and Pd(PPh₃)₂Cl₂ (0.4 g, 0.58 mmol) was prepared. Redistilled toluene (200 mL) was subsequently poured in the mixture, then stirring the mixture to reflux under nitrogen (N_2) atmosphere for 5 h. Following this, the mixture was hot-filtered utilizing silica gel column and subsequently concentrated to dryness, resulting in a white solid. (11.8 g, 77 %)



Scheme 1. Procedure for the synthesis of DMID-BP and BFCz-BP.

2.1.7. Synthesis of 7-(4-(7,7-dimethylindeno [2,1-b]carbazol-5(7H)-yl)phenyl)benzo [4,5]imidazo [1,2-f]phenanthridine (DMID-BP)

The reactants IN2 (5 g, 16.51 mmol), IM3 (8.4 g, 17.34 mmol), K_2CO_3 (3.42 g, 24.76 mmol), toluene (30 mL), ethanol (15 mL), H_2O (15 mL), catalyst $\text{Pd}(\text{OAc})_2$ (0.15 g, 2 wt%) and X-phos (0.30 g, 4 wt%) were introduced in a three-necked flask. Then stirring the mixture to reflux under nitrogen (N_2) atmosphere for 2 h. After cooling, filtration,

recrystallization, washing and drying, the resulting pure product was a white powder. The final solid was 9.3 g, representing an 90 % yield.

2.1.8. Synthesis of 5-(4-(benzo [4,5]imidazo [1,2-f]phenanthridin-7-yl)phenyl)-5H-benzofuro [3,2-c]carbazole (BFCz-BP)

The reactants IN2 (5 g, 16.51 mmol), IM4 (7.9 g, 17.34 mmol), K_2CO_3 (3.42 g, 24.76 mmol), toluene (30 mL), ethanol (15 mL), H_2O (15

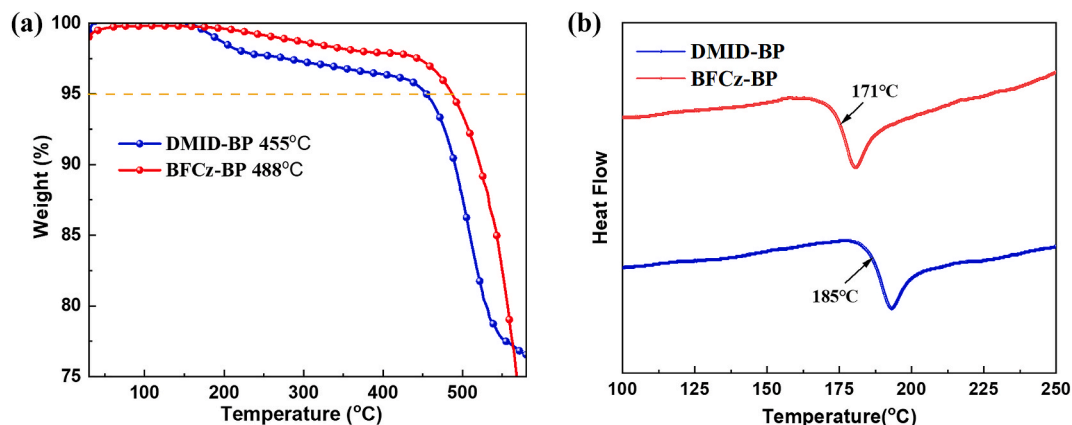


Fig. 1. Results from TGA (a) and DSC (b) on DMID-BP and BFCz-BP.

Table 1
Properties of DMID-BP and BFCz-BP.

Compound	λ^a abs,max (nm)	λ^a PL (nm)	λ^a Phos (nm)	E^c T(eV)	E^b g(eV)	HOMO ^d (eV)	LUMO ^e (eV)	T ^f d(°C)	T ^f g(°C)
DMID-BP	302	431	492	2.52	3.21	-5.51	-2.30	455	185
BFCz-BP	353	413	489	2.53	3.24	-5.71	-2.47	488	171

^a Tests were conducted in a tetrahydrofuran (THF) solution (1×10^{-5} M), with the results sourced from UV-vis absorption, photoluminescence (PL), phosphorescence spectra.

^b Determined by the onset of absorption spectra, $E_g = 1241/\lambda_{\text{onset}}$.

^c E_T determined by phosphorescence spectra at 77 k.

^d HOMO energy levels computed using $E_{\text{HOMO}} = -(E_{\text{OX onset}} + 4.4)$.

^e LUMO energy levels computed using $E_{\text{LUMO}} = E_{\text{HOMO}} + E_g$.

^f Measured through DSC and TGA tests.

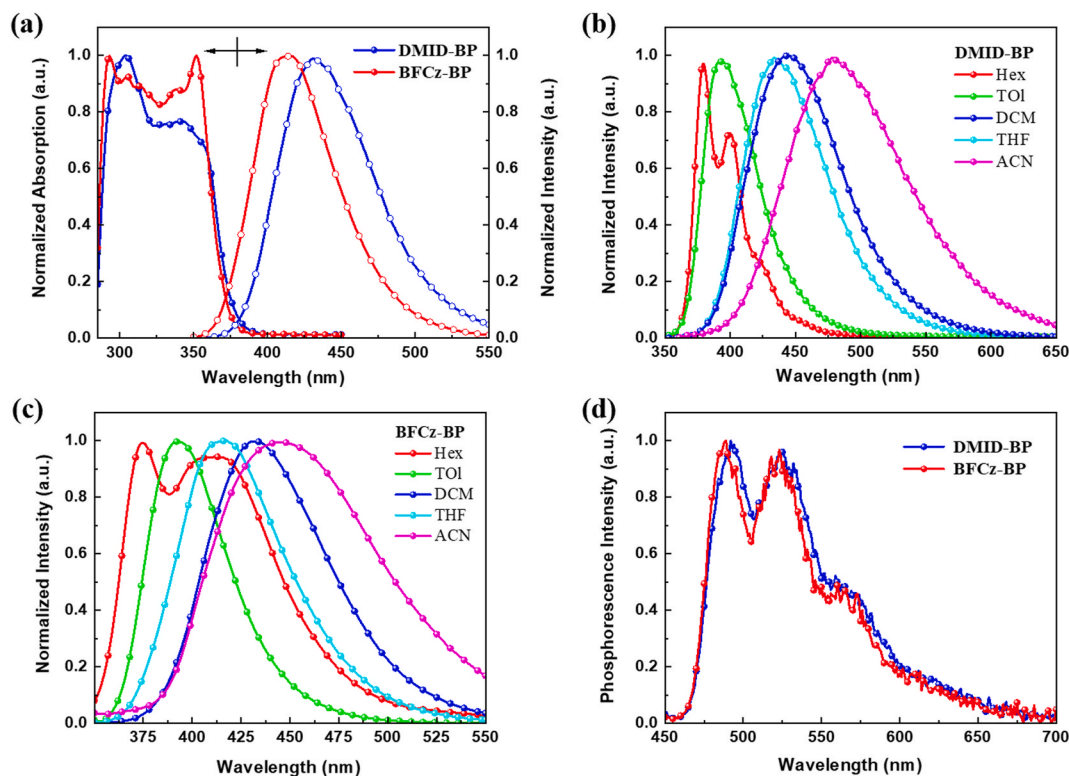


Fig. 2. (a) UV-Vis and PL spectra in THF; (b) DMID-BP and (c) BFCz-BP PL spectra in solvents with different polarities, along with (d) low-temperature phosphorescence spectra (2-Me-THF). Measurement concentration: 10^{-5} M.

mL), catalyst Pd(OAc)₂ (0.15 g, 2 wt%) and ligand X-phos (0.30 g, 4 wt %) were introduced in a three-necked flask. Then stirring the mixture to reflux under nitrogen (N₂) atmosphere for 2 h. After cooling, filtration, recrystallization, washing and drying, the resulting pure product was a white powder. The final solid was 8.7 g, representing an 88 % yield.

3. Results and discussions

3.1. Synthesis and characterization

The synthesis route of DMID-BP and BFCz-BP are shown in Scheme 1. The successful synthesis of the two target compounds was accomplished through the Suzuki coupling reaction, with a subsequent straightforward purification. All products were comprehensively characterized using ¹H nuclear magnetic resonance (¹H NMR), ¹³C NMR, and mass spectrometry (MS). The results are presented in Fig. S1–15.

3.2. Thermal properties

Excellent thermal stability of OLED materials plays a key role in the

formation of high-quality thin films, which in turn enhances the device stability. Thermogravimetric analysis (TGA) and differential scanning calorimetry (DSC) were employed to determine the thermal degradation temperature (T_d, weight loss of 5 %) and glass transition temperature (T_g) of the two compounds, thereby assessing their thermal robustness. Fig. 1 presents the corresponding TGA and DSC results, and the pertinent data are outlined in Table 1. Both DMID-BP and BFCz-BP demonstrate high thermal stability, characterized by T_d of 455 °C and 488 °C, respectively. Compared to the previously reported benzimidazole-hybridized phenanthridine-based (BP-based) emitting materials, these values are considerably higher. The enhanced thermal stability of DMID-BP and BFCz-BP can be attributed to their larger planar rigid structures in the hole transport units, which effectively improve the morphological stability of these compounds. Concurrently, the T_g for DMID-BP and BFCz-BP, is determined from their DSC curves, as 185 °C and 171 °C, respectively. The superior thermal properties of DMID-BP and BFCz-BP are deemed sufficient for practical applications.

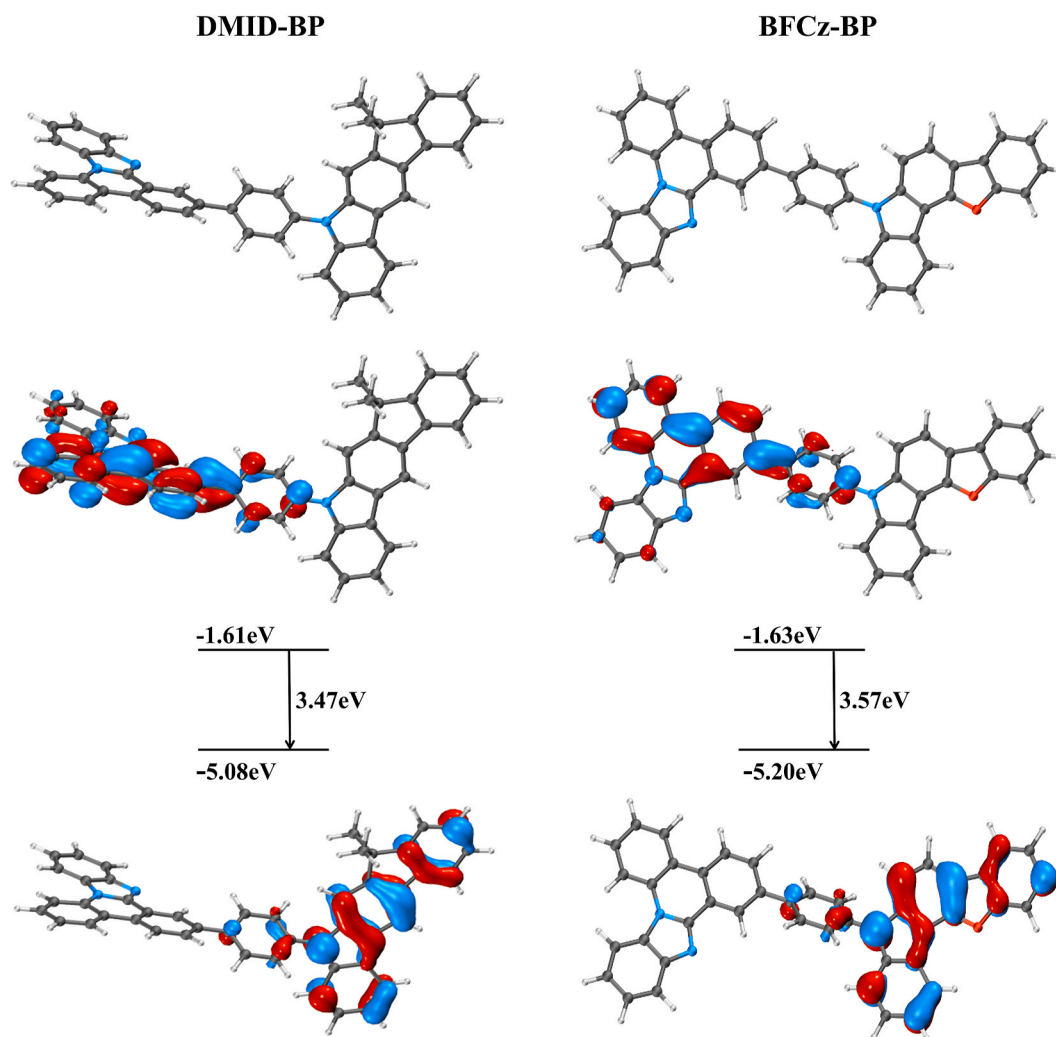


Fig. 3. HOMO, LUMO distribution and bandgap of DMID-BP and BFCz-BP.

3.3. Photophysical properties

The ultraviolet–visible (UV–vis) absorption and photoluminescence

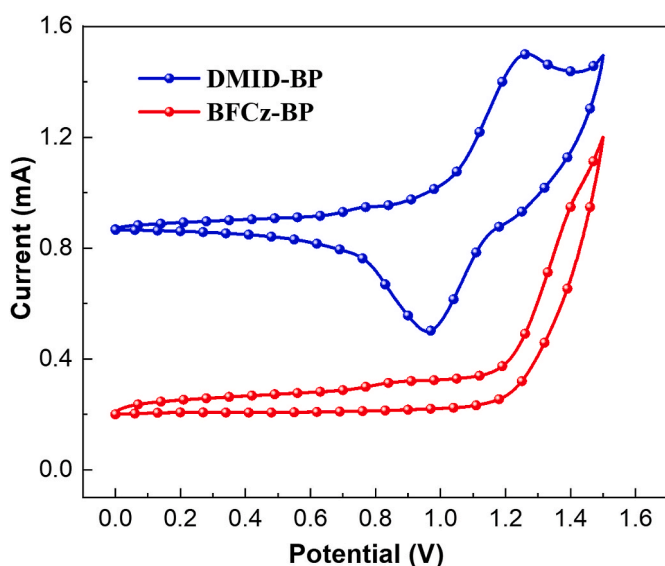


Fig. 4. CV curves of DMID-BP and BFCz-BP.

(PL) spectra of compounds **DMID-BP** and **BFCz-BP** in tetrahydrofuran, low-temperature phosphorescence spectra recorded at 77 K, are presented in Fig. 2. The UV–vis absorption spectrum of **BFCz-BP** displayed well-defined and sharp peaks (Fig. 2 a). The two absorption bands of both compounds around 300 nm were ascribed to local π - π^* transitions. In the absorption spectrum of the **BFCz-BP**, the phenyl carbazole skeleton exhibits a sharp peak between 325 nm and 360 nm, whereas in **DMID-BP**, it appears as a shoulder peak. In tetrahydrofuran solution, both compounds exhibit blue fluorescence, with an obvious emission peak around 436 nm. Based on the absorption onset, it was determined that the optical energy gaps (E_g) of **DMID-BP** and **BFCz-BP** were 3.21 eV and 3.24 eV, respectively. The influence of solvent polarity on **DMID-BP** and **BFCz-BP** was examined using their PL spectra to further explore the nature of their excited states (Fig. 2b and c). As the solvent polarity increases, a notable redshift is observed in the maximum absorption peaks, shifting from 380 nm to 480 nm and from 380 nm to 450 nm, respectively. The more significant redshift observed for **DMID-BP** compared to **BFCz-BP** in DCM suggests a stronger intramolecular charge transfer (ICT) effect, which can be explained by the better electron-donating capability of the indolocarbazole unit over the benzofurocarbazole unit. In addition, with the increase in solvent polarity, the fine construction of the PL spectra slowly diminishes, and the full width at half maximum (FWHM) broadens. This behavior further supports the conclusion that both compounds exhibit ICT characteristics. Furthermore, the phosphorescence spectra (Fig. 2 d) of **DMID-BP** and **BFCz-BP** were measured at 77 K to determine their E_T . The calculated E_T

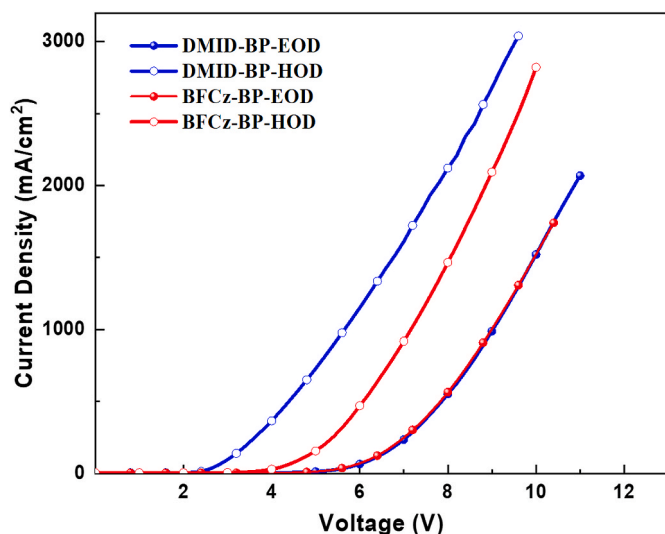


Fig. 5. J-V profiles of HODs, EODs for DMID-BP and BFCz-BP.

values for both materials were found to be 2.52 eV and 2.53 eV, respectively, making them promising candidates for host-guest doping structures in red PhOLEDs.

3.4. Theoretical calculations and electrochemical properties

Density functional theory (DFT) calculations at the B3LYP/6-31G(d) level using Gaussian 09 were conducted to have a comprehension on the electronic properties of DMID-BP and BFCz-BP [32]. These two compounds exhibit nearly identical HOMO and LUMO distributions. As shown in Fig. 3, the LUMO is primarily localized on the BP unit, with slightly delocalization extending to the adjacent phenyl group. As for the HOMO, the primary location of it is on the indolocarbazole unit in DMID-BP and on the benzofurocarbazole unit in BFCz-BP. The distinct separation of HOMO and LUMO levels enables efficient mobility of both holes and electrons, making DMID-BP and BFCz-BP promising bipolar host materials [33].

Charge carrier transport in OLEDs involves repeated oxidation and reduction processes of the materials. Thus, cyclic voltammetry (CV) was used to examine the electrochemical properties of DMID-BP and BFCz-BP in DCM solutions (see Fig. 4). Based on the onset potential of their first oxidation wave (E_{ox} onset), the HOMO energy levels of the two materials were calculated as -5.51 eV and -5.71 eV, respectively. The LUMO energy levels of DMID-BP and BFCz-BP were determined by combining their respective HOMO levels with the E_g, resulting in -2.30 eV and -2.47 eV, respectively.

3.5. Carrier transport properties

Since charge carrier balance within the emitting layer is a critical factor for achieving high performance in OLEDs, the charge transport capability of DMID-BP and BFCz-BP were evaluated by fabricating hole-

only devices (HODs) and electron-only devices (EODs). The construction of HODs was [ITO/MoO₃ (3 nm)/NPB (5 nm)/host (50 nm)/NPB (5 nm)/Al (80 nm)], while the corresponding configurations for EODs was [ITO/TPBi (10 nm)/host (45 nm)/TPBi (10 nm)/LiF (10 nm)/Al (80 nm)]. Seen from Fig. 5, all single-carrier devices exhibited a high current density at low voltage, demonstrating that both compounds possess excellent bipolar characteristics. It is noteworthy that DMID-BP demonstrated stronger hole-transporting ability compared to BFCz-BP. It is probably because the two methyl units in DMID, which are attached an aromatic ring. These methyl groups can raise the HOMO energy level by donating electron density to the π -system thus lead to an improved hole injection and transport in OLED devices. However, BFCz-BP generally exhibits more balanced hole- and electron-transporting properties.

3.6. Electroluminescence properties

The electroluminescent (EL) performance of four diodes is presented in Figs. 7 and 8, with the corresponding data compiled in Table 2.

3.6.1. Red PhOLEDs based on DMID-BP and BFCz-BP

To estimate the electroluminescent (EL) properties of DMID-BP and BFCz-BP, red PhOLEDs have been fabricated first. The devices configuration is as follows: ITO/MoO₃ (3 nm)/NPB (40 nm)/TCTA (10 nm)/DMID-BP or BFCz-BP: 5 wt% Ir(piq)₂acac (20 nm)/TPBi (40 nm)/LiF (1 nm)/Al (100 nm). TCTA was used as the electron blocking layer, ITO and Al functions as the anode and cathode, respectively. NPB and TPBi are acted as hole- and electron-transporting layers, while MoO₃ and LiF serves as hole- and electron-injection layers, respectively. DMID-BP and BFCz-BP were doped with Ir(piq)₂acac to fabricate the emitting layer for devices R1 and R2, respectively. Diagrams of energy levels for the green and red diodes, architecture of the green and red devices along with materials' molecular structures utilized in the devices are depicted in Fig. 6.

The EL spectra of red PhOLEDs were investigated, as illustrated in Fig. 7 a. Devices R1 and R2 display a strong red emission located at 622 nm, indicating efficient energy transfer from the host material to the emitter and well-confined triplet excitons in the emitting layer (EML). Their respective CIE chromaticity coordinates (x, y), (0.661, 0.310) and (0.657, 0.308), meet the National Television Systems Committee (NTSC) standard requirements. As expected, the two devices demonstrate relatively high light-emitting efficiency with minimal roll-off efficiency. Notably, the maximum external quantum efficiency (EQE_{max}) of R1 and R2 reaches 23.68 % and 20.26 %, respectively, and these values are significantly superior to those reported for majority of red PhOLEDs [34, 35]. The luminance of R1 reached 52.4 cd/m² at a voltage of 2.80 V, corresponding to its turn-on voltage. Besides, device R1 shows a high maximum current efficiency ($\eta_{c,max}$) of 21.20 cd/A, a maximum power efficiency ($\eta_{p,max}$) of 23.77 lm/W, and a peak luminance (L_{max}) of 10071.27 cd/m², while device R2 shows a $\eta_{c,max}$ of 18.09 cd/A, a $\eta_{p,max}$ of 18.63 lm/W, a L_{max} of 7153.52 cd/m² and a V_{on} of 2.92 V. The higher EQE_{max} and lower turn-on voltages of R1 can be ascribed to the enhanced hole transport capabilities of DMID-BP at a low driving voltage. Additionally, the EQE of R2 reaches 19.18 % at a luminance of

Table 2
Red and green device EL characteristics.

Device	λ^a EL(nm)	V ^b on(V)	EQE ^c max(%)	η^c c,max(cd/A)	η^c p,max(lm/W)	L ^c max(cd/m ²)	CIE ^b (x,y)
R1	622	2.80	23.68	21.20	23.77	10071.3	(0.661,0.310)
R2	622	2.92	20.26	18.10	18.63	7153.5	(0.657,0.308)
G1	525	2.80	17.23	65.89	73.88	24061.4	(0.308,0.632)
G2	525	2.93	13.27	49.22	53.21	18521.8	(0.305,0.622)

^a EL spectra measured at 5 V.

^b Turn-on voltage at 1 cd/m².

^c The maximum external quantum efficiency, current efficiency, power efficiency, and luminance.

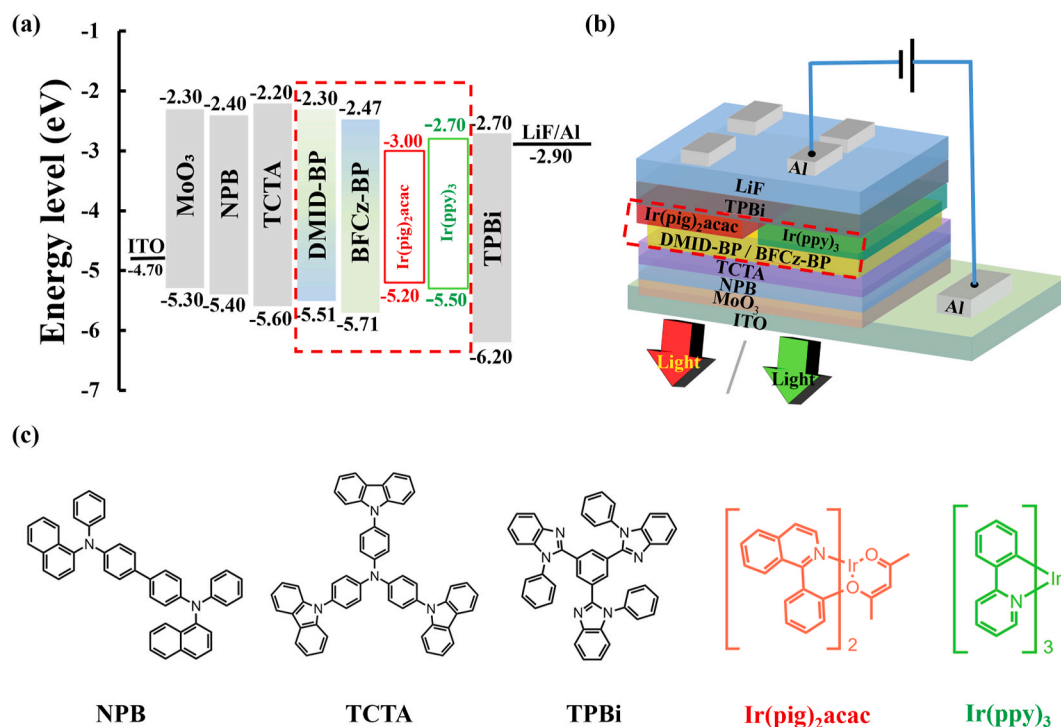


Fig. 6. (a) Diagrams of energy levels for the red and green diodes. (b) architecture of the red and green diodes. (c) Materials' molecular structures utilized in the diodes. (For interpretation of the references to color in this figure legend, the reader is referred to the Web version of this article.)

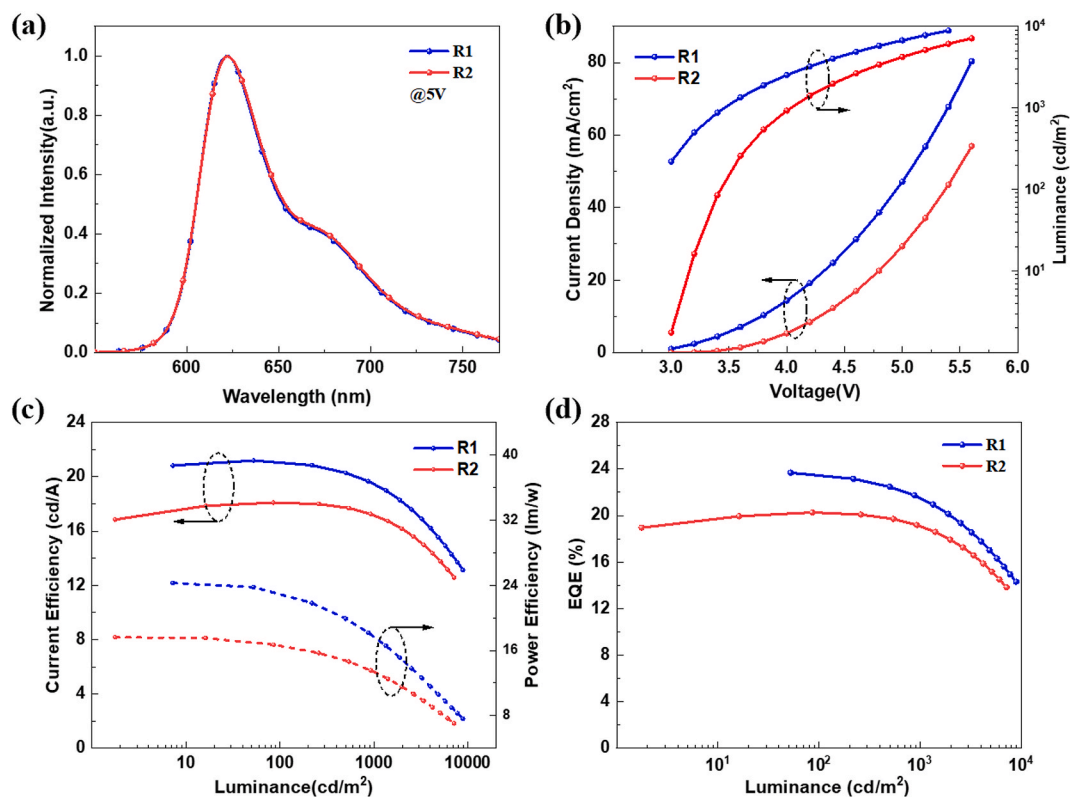


Fig. 7. (a) Normalized EL data (5 V) (b) J-V-L (c) PE-L-CE (d) EQE-L profiles.

1000 cd/m², indicating that the device exhibits small efficiency roll-off. Furthermore, the meticulously optimized device architecture ensures that the HOMO/LUMO energy levels of DMID-BP and BFCz-BP align well with those of the neighboring layers. Over time, R2 exhibited a

slower rate of luminance degradation, which can be attributed to the more balanced charge carrier transport properties of BFCz-BP, thereby enhancing the device's operational stability (Fig. S18). In general, DMID-BP and BFCz-BP are effective host materials for red PhOLEDs.

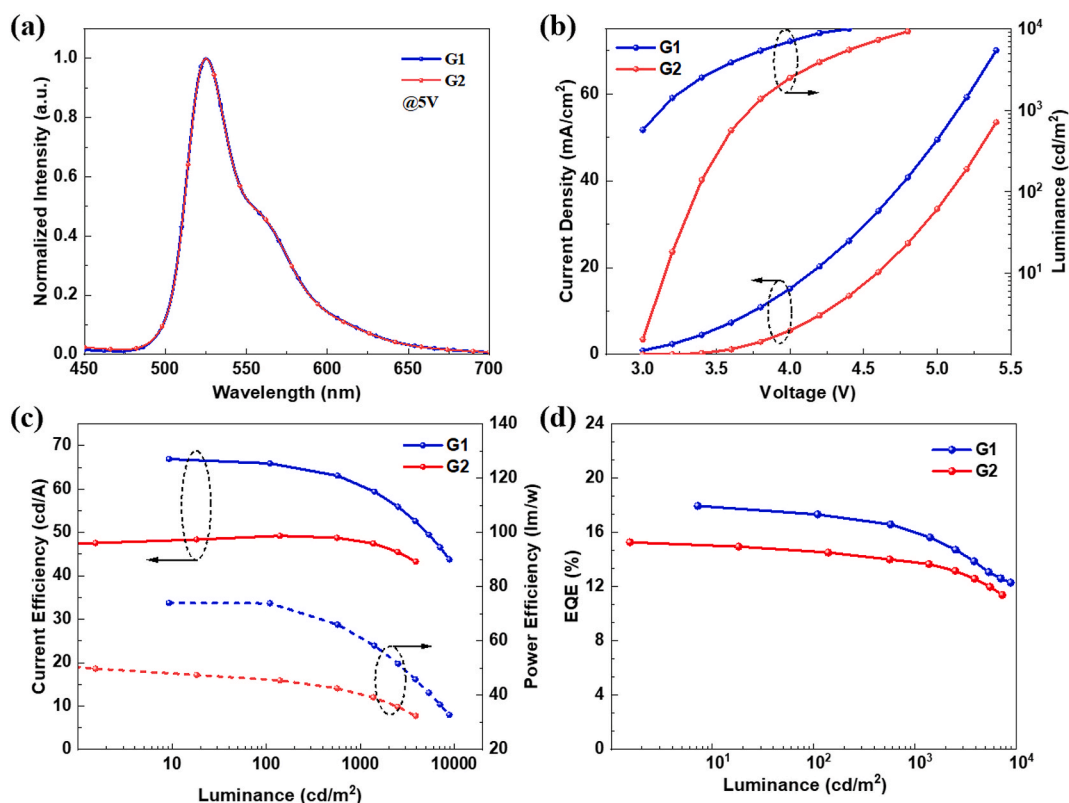


Fig. 8. (a) Normalized EL data (5 V) (b) J-V-L (c) PE-L-CE (d) EQE-L profiles.

3.6.2. Green PhOLEDs based on DMID-BP and BFCz-BP

Moreover, since DMID-BP and BFCz-BP exhibited excellent performance in red PhOLEDs, we explored their potential by fabricating green PhOLEDs using these two compounds. The device architecture consisted of ITO/MoO₃ (3 nm)/NPB (40 nm)/TCTA (10 nm)/DMID-BP or BFCz-BP: Ir(ppy)₃ (7 wt%, 20 nm)/TPBi (40 nm)/LiF (1 nm)/Al (100 nm). Fig. 8 illustrates the optoelectronic characteristics of the two devices. Under an operating voltage of 5 V, both devices G1 and G2 demonstrate maximum emission peaks at wavelengths of 525 nm, with correlative CIE coordinates of (0.308, 0.632) and (0.305, 0.622), respectively. Additionally, G1 presented pure green electroluminescence with EQE_{max} of 17.23 %. As the driving voltage increases, the EL spectra of the four diodes remained almost consistent (Fig. S17), indicating their excellent stability during the charge injection process.

4. Conclusion

In summary, two bipolar host materials with a D- π -A structure were built, where DMID and BFCz act as the hole-transporting units, benzene serves as the π -bridge, and BP functions as the electron-transporting moiety. The introduction of DMID and BFCz greatly elevated the thermal properties, carrier mobility, and facilitated the achievement of suitable HOMO/LUMO energy levels. DFT calculations confirm a distinct separation between the HOMO and LUMO levels, indicating that the material exhibits commendable bipolar properties and effectively facilitates carrier transport within the luminescent layer. More encouragingly, the red devices based on DMID-BP and BFCz-BP demonstrated impressive performance, achieving EQE_{max} values of 23.68 % and 20.26 %, respectively. Those results suggest that these bipolar host materials based on DMID and BFCz hold significant promise for application in OLEDs with ultra-high efficiency.

CRediT authorship contribution statement

Minzhen Li: Writing – original draft, Methodology, Formal analysis, Data curation. **Yong Yang:** Resources, Investigation, Data curation. **Sisi Lan:** Validation, Methodology. **Yingyi Wei:** Software, Investigation. **Zhi Zhang:** Supervision. **Haitao Zhou:** Writing – review & editing, Validation. **Zhiyun Zhang:** Supervision, Project administration. **Jinhai Huang:** Funding acquisition, Conceptualization. **Zhenyuan Xia:** Writing – review & editing, Supervision.

Declaration of competing interest

The authors declare that they have no known competing financial interests or personal relationships that could have appeared to influence the work reported in this paper.

Appendix A. Supplementary data

Supplementary data to this article can be found online at <https://doi.org/10.1016/j.dyepig.2025.112882>.

Data availability

No data was used for the research described in the article.

References

- [1] Tang CW, VanSlyke SA. Organic electroluminescent diodes. Appl Phys Lett 1987; 51:913–5. <https://doi.org/10.1063/1.98799>.
- [2] Baldo MA, O'Brien DF, You Y, Shoustikov A, Sibley S, Thompson ME, et al. Highly efficient phosphorescent emission from organic electroluminescent devices. Nature 1998;395:151–4. <https://doi.org/10.1038/25954>.
- [3] Xiao L, Chen Z, Qu B, Luo J, Kong S, Gong Q, et al. Recent progresses on materials for electrophosphorescent organic light-emitting devices. Adv Mater 2011;23: 926–52. <https://doi.org/10.1002/adma.201003128>.

- [4] Li W, Zhang H, Shi S, Xu J, Qin X, He Q, et al. Recent progress in silver nanowire networks for flexible organic electronics. *J Mater Chem C* 2020;8:4636–74. <https://doi.org/10.1039/C9TC06865A>.
- [5] Hong G, Gan X, Leonhardt C, Zhang Z, Seibert J, Busch JM, et al. A brief history of OLEDs-Emitter development and industry milestones. *Adv Mater* 2021;33:e2005630. <https://doi.org/10.1002/adma.202005630>.
- [6] Aydemir M, Haykr G, Battal A, Jankus V, Sugunan SK, Dias FB, et al. High efficiency OLEDs based on anthracene derivatives: the impact of electron donating and withdrawing group on the performance of OLED. *Org Electron* 2016;30:149–57. <https://doi.org/10.1016/j.orgel.2015.11.026>.
- [7] Xu J, Liu H, Li J, Zhao Z, Tang B. Multifunctional bipolar materials serving as emitters for efficient deep-blue fluorescent OLEDs and as hosts for phosphorescent and white OLEDs. *Adv Opt Mater* 2021;9:2001840.
- [8] Li MT, Qu ZH, Liu R, Yang YJ, Zuo P, Liao LS, et al. Acceptor- σ -donor- σ -acceptor host material for red phosphorescent and thermally activated delayed fluorescent OLEDs. *Org Electron* 2024;130:107072. <https://doi.org/10.1016/j.orgel.2024.107072>.
- [9] Yin Z, Gu M, Ma H, Jiang X, Zhi J, Wang Y, et al. Molecular engineering through control of structural deformation for highly efficient ultralong organic phosphorescence. *Angew Chem Int Ed Engl* 2021;60:2058–63. <https://doi.org/10.1002/anie.202011830>.
- [10] Wei Q, Fei N, Islam A, Lei T, Hong L, Peng R, et al. Small-molecule emitters with high quantum efficiency: mechanisms, structures, and applications in OLED devices. *Adv Opt Mater* 2018;6:1800512. <https://doi.org/10.1002/adom.201800512>.
- [11] Hu S, Zeng J, Zhu X, Guo J, Chen S, Zhao Z, et al. Universal bipolar host materials for blue, green, and red phosphorescent OLEDs with excellent efficiencies and small-efficiency roll-off. *ACS Appl Mater Interfaces* 2019;11:27134–44. <https://doi.org/10.1021/acsami.9b06995>.
- [12] Patil VV, Lee KH, Lee HJ. 11,11-Dimethyl-11H-indeno[1,2-b]indolo[1,2,3-jk]carbazole: a rigid chromophore with novel amalgamation strategy for long lifetime blue fluorescent organic light-emitting diodes. *Chem Eng J* 2020;395:125125. <https://doi.org/10.1016/j.cej.2020.125125>.
- [13] Weaver MS, Fusella MA, Saramak R, Bushati R, Mundoor H, Menon VM, et al. Plasmonic PhOLEDs: increasing OLED stability. *J Mater Chem C* 2022;10:4182–6. <https://doi.org/10.1039/d1tc05674c>.
- [14] Li DL, Liu D, Li JY, Dong RZ, Liu BT, Wei QH. Low-driving-voltage sky-blue phosphorescent organic light-emitting diodes with bicarbazole-bipyridine bipolar host materials. *Mater Chem Front* 2021;5:2867–76. <https://doi.org/10.1039/d1qm00018g>.
- [15] Lee J, Chopra N, Eom SH, Zheng Y, Xue JG, So F, et al. Effects of triplet energies and transporting properties of carrier transporting materials on blue phosphorescent organic light emitting devices. *Appl Phys Lett* 2008;93:123306. <https://doi.org/10.1063/1.2978235>.
- [16] Zassowski P, Ledwon P, Kurowska A, Herman AP, Lapkowski M, Cherpak V, et al. 1,3,5-Triazine and carbazole derivatives for OLED applications. *Dyes Pigments* 2018;149:804–11. <https://doi.org/10.1016/j.dyepig.2017.11.040>.
- [17] Yang X, Zhou G, Wong WY. Functionalization of phosphorescent emitters and their host materials by main-group elements for phosphorescent organic light-emitting devices. *Chem Soc Rev* 2015;44:8484–575. <https://doi.org/10.1039/c5cs00424a>.
- [18] Ito T, Sasabe H, Nagai Y, Watanabe Y, Onuma N, Kido J. A series of dibenzofuran-based n-Type exciplex host partners realizing high-efficiency and stable deep-red phosphorescent OLEDs. *Chemistry* 2019;25:7308–14. <https://doi.org/10.1002/chem.201805907>.
- [19] Liu C, Li T, Sun M, Xie M, Zhou Y, Feng W, et al. Host material for multi-color display with high and stable electro-phosphorescent efficiencies: meta-linkage for balanced hole and electron injection. *Adv Funct Mater* 2023;33:2215066. <https://doi.org/10.1002/adfm.202215066>.
- [20] Chu LZ, Ma CL, Zhang L, Zhou YN, Song JR, Sun QK, et al. Multifunctional oxadiazole-based ultraviolet-emitting materials used as hosts for multicolor phosphorescence. *Chem Sci* 2025;16(12):5252–9. <https://doi.org/10.1039/D5SC00374A>.
- [21] Zhou DD, Zhang BQ, Yu ZY, Liao Q, Fu HB. tert-Butyl-substituted bicarbazole as a bipolar host material for efficient green and yellow PhOLEDs. *New J Chem* 2020;44:10472–8. <https://doi.org/10.1039/d0nj01210f>.
- [22] Wang SN, Qi HY, Huang H, Li J, Liu YC, Xue SF, et al. Asymmetric deep-blue tetrafluorobenzene-bridged fluorophores with hybridized local and charge-transfer characteristics for efficient OLEDs with low efficiency roll-off. *Mater Chem Front* 2024. <https://doi.org/10.1039/d4qm00636d>.
- [23] Meng ZM, Zhu YN, Li HY, Zhang XP, Shang YF, Kuang CC, et al. Highly efficient and stable pure-red phosphorescent organic light-emitting diodes based on heptacyclic bipolar hosts featuring an armor-like structure. *J Mater Chem C* 2024;12:9993–8. <https://doi.org/10.1039/d4tc01313a>.
- [24] Tan Y, Zhao Z, Shang L, Liu Y, Wei C, Li J, et al. A novel bipolar D- π -A type phenanthroimidazole/carbazole hybrid material for high efficiency nonpopped deep-blue organic light-emitting diodes with NTSC CIEy and low efficiency roll-off. *J Mater Chem C* 2017;11901–9. <https://doi.org/10.1039/c7tc04089j>.
- [25] Song W, Chen Y, Xu Q, Mu H, Cao J, Huang J, et al. [1,2,4]Triazole[1,5-a]pyridine-Based Host Materials for Green Phosphorescent and Delayed-Fluorescence OLEDs with Low Efficiency Roll-Off. *ACS Appl Mater Interfaces* 2018;10:24689–98. <https://doi.org/10.1021/acsami.8b07462>.
- [26] Rodella F, Bagnich S, Duda E, Meier T, Kahle J, Athanasopoulos S, et al. High triplet energy host materials for blue TADF OLEDs-A tool box approach. *Front Chem* 2020;8:657. <https://doi.org/10.3389/fchem.2020.00657>.
- [27] Patil VV, Lim J, Lee JY. Strategic synchronization of 7,7-Dimethyl-5,7-dihydroindeno[2,1-b]carbazole for narrow-band, pure violet organic light-emitting diodes with an efficiency of > 5% and a CIE y coordinate of < 0.03. *ACS Appl Mater Interfaces* 2021;13:14440–6. <https://doi.org/10.1021/acsami.1c02635>.
- [28] Li N, Zhao JL, Wang Y, Wang S, Feng KR, Wu JY, et al. Efficient interaction of indeno carbazole and alkoxy side chains with enormous differences in polarity achieve highly conductive and longevous anion exchange membranes. *J Membr Sci* 2024;701:122761. <https://doi.org/10.1016/j.memsci.2024.122761>.
- [29] Song XG, Shen SG, Zou SN, Guo FY, Gao SY, Wang Y, et al. Asymmetric strategy based on 5H-benzofuro[3,2-c]carbazole enables efficient narrowband multi-resonance thermally activated delayed fluorescence emitters. *J Mater Chem C* 2023;11:16928–32. <https://doi.org/10.1039/d3tc02902f>.
- [30] Gong MS, Cha JR, Lee CW. Synthesis and device properties of mCP analogues based on fused-ring carbazole moiety. *Org Electron* 2017;42:66–74. <https://doi.org/10.1016/j.orgel.2016.12.027>.
- [31] Yang Y, Zhang DQ, Wu ZX, Zhou HT, Huang JH, Guo LF, et al. Novel bipolar host materials based on benzimidazole-hybridized phenanthridine for efficient red PhOLEDs. *Dyes Pigments* 2024;230:112322. <https://doi.org/10.1016/j.dyepig.2024.112322>.
- [32] Lu T, Chen FW. Multiwfn: a multifunctional wavefunction analyzer. *J Comput Chem* 2012;33:580–92.
- [33] Li J, Zhang T, Liang Y, Yang R. Solution-processible carbazole dendrimers as host materials for highly efficient phosphorescent organic light-emitting diodes. *Adv Funct Mater* 2013;23:619–28.
- [34] Wu HF, Wang G, Zhang DQ, Jin X, Luo X, Guo SY, et al. Novel carbazole- and dioxino[2,3-b]pyrazine-based bipolar hosts for red PhOLEDs with a high brightness. *New J Chem* 2022;46:12703–10. <https://doi.org/10.1039/d2nj01951e>.
- [35] Hu YT, Yang XD, Huang ZT, Xie QY, Chen YH, Zheng YQ, et al. D-A-D-type bipolar hosts incorporating N-phenylcarbazole and quinoline at various connection sites with high electron mobility for red electrophosphorescence. *Synth Met* 2024;308:117712. <https://doi.org/10.1016/j.synthmet.2024.117712>.